Available online at www.sciencedirect.com

ScienceDirect

Neuromuscular Disorders 31 (2021) 56–68

www.elsevier.com/locate/nmd

Impaired NDRG1 functions in Schwann cells cause demyelinating neuropathy in a dog model of Charcot-Marie-Tooth type 4D

Fredrik S. Skedsmo[a,*], Arild Espenes[b], Michael A. Tranulis[b], Kaspar Matiasek[c], Gjermund Gunnes[b], Inge Bjerkås[b], Lars Moe[a], Susan Skogtvedt Røed[b], Mette Berendt[d], Merete Fredholm[e], Cecilia Rohdin[f,g], G. Diane Shelton[h], Per Bruheim[i], Marit H. Stafsnes[i], Zdenka Bartosova[i], Lene C. Hermansen[j], Øyvind Stigen[a], Karin H. Jäderlund[a]

[a] *Department of Companion Animal Clinical Sciences, Faculty of Veterinary Medicine, Norwegian University of Life Sciences, Ullevålsveien 72, 0454 Oslo, Norway*

[b] *Department of Preclinical Sciences and Pathology, Faculty of Veterinary Medicine, Norwegian University of Life Sciences, Ullevålsveien 72, 0454 Oslo, Norway*

[c] *Section of Clinical & Comparative Neuropathology, Centre for Clinical Veterinary Medicine, Ludwig-Maximilians-Universität, Veterinärstr. 13, D-80539 Munich, Germany*

[d] *Department of Veterinary Clinical Sciences, Faculty of Health and Medical Sciences, University of Copenhagen, Dyrlægevej 16, 1870 Frederiksberg C, Denmark*

[e] *Department of Veterinary and Animal Sciences, Faculty of Health and Medical Sciences, University of Copenhagen, Grønnegårdsvej 2, 1870 Frederiksberg C, Denmark*

[f] *Department of Clinical Sciences, Swedish University of Agricultural Sciences, Ultunaalléen 5A, 756 51 Uppsala, Sweden*

[g] *Anicura Albano Small Animal Hospital, Rinkebyvägen 21, 182 36 Danderyd, Sweden*

[h] *Department of Pathology, School of Medicine, University of California San Diego, 9500 Gilman Drive, La Jolla, California 92093-0709, United States of America*

[i] *Department of Biotechnology and Food Science, Faculty of Natural Sciences, Norwegian University of Science and Technology, Sem Sælands vei 6, 7034 Trondheim, Norway*

[j] *Department of Plant Sciences, Faculty of Biosciences, Norwegian University of Life Sciences, Universitetstunet 3, 1433 Ås, Norway*

Received 17 April 2020; received in revised form 13 November 2020; accepted 18 November 2020

Abstract

Mutations in the N-myc downstream-regulated gene 1 (*NDRG1*) cause degenerative polyneuropathy in ways that are poorly understood. We have investigated Alaskan Malamute dogs with neuropathy caused by a missense mutation in *NDRG1*. In affected animals, nerve levels of NDRG1 protein were reduced by more than 70% ($p < 0.03$). Nerve fibers were thinly myelinated, loss of large myelinated fibers was pronounced and teased fiber preparations showed both demyelination and remyelination. Inclusions of filamentous material containing actin were present in adaxonal Schwann cell cytoplasm and Schmidt-Lanterman clefts. This condition strongly resembles the human Charcot-Marie-Tooth type 4D. However, the focally folded myelin with adaxonal infoldings segregating the axon found in this study are ultrastructural changes not described in the human disease. Furthermore, lipidomic analysis revealed a profound loss of peripheral nerve lipids. Our data suggest that the low levels of mutant NDRG1 is insufficient to support Schwann cells in maintaining myelin homeostasis.

Keywords: Alaskan Malamute; Canine; CMT; Greyhound; N-myc downstream-regulated gene 1; Polyneuropathy.

1. Introduction

Degenerative neuropathies caused by mutations in *N-myc downstream-regulated gene 1* (*NDRG1*) are reported from

* Corresponding author.
E-mail address: Fredrik.strebel.skedsmo@nmbu.no (F.S. Skedsmo).

https://doi.org/10.1016/j.nmd.2020.11.010

humans, classified as Charcot-Marie-Tooth type 4D (CMT4D) [1], Greyhound show dogs [2] and Alaskan Malamute dogs [3]. Cases of Alaskan Malamute polyneuropathy (AMP) were first described in Norway in the 1980′s [4] and the disease was believed eradicated due to breeding programs, but re-emerged in Scandinavia several decades later [3]. AMP is inherited in an autosomal recessive manner and associated with a missense mutation in *NDRG1* (p.Gly98Val) [3]. Clinically, the disease is slowly progressive and characterized by tetraparesis, pelvic limb ataxia, exercise intolerance and inspiratory stridor with onset of clinical signs in adolescence [3-5].

The NDRG1 protein is not specific for peripheral nerves and is detected in a wide variety of human, rodent and dog tissues with the highest levels in epithelial cells and myelinating glial cells [6–8]. Still, how *NDRG1* mutations lead to neuropathies without clinical signs from other body systems, as well as the specific function of NDRG1 in the peripheral nervous system, are not clear [8,9]. The protein is functionally diverse being involved in several cellular processes, such as vesicular transport [10–12], microtubule dynamics [13], centrosome homeostasis [14] and lipid metabolism [15,16]. The posttranslational processing of NDRG1 is complex and tissue- and cell-specific [7]. Notably, in myelinating Schwann cells high levels of phosphorylated NDRG1 localize to the abaxonal cytoplasm and outer parts of the Schmidt-Lanterman clefts [7,17]. In addition to its role in neuropathies, the NDRG1 protein is also reported to be involved in carcinogenesis [18], metastasis suppression [19] and counteracts epithelial-mesenchymal transition [20].

Charcot-Marie-Tooth disease (CMT) denominates the most frequent forms of inherited neuropathies in humans. This is a heterogeneous group of diseases, further classified into subtypes based on clinical and pathological phenotype, mode of inheritance, nerve conduction velocity and causative gene [21]. The CMT4 subgroup includes demyelinating neuropathies with autosomal recessive inheritance [22]. One of them, CMT4D, also known as Hereditary motor and sensory neuropathy-Lom (HMSNL), is a primary demyelinating neuropathy with onion bulb formation, accumulation of pleomorphic material in the Schwann cell cytoplasm and secondary axonal loss [23]. In contrast, the *NDRG1*-associated polyneuropathy of Greyhound show dogs was reportedly dominated by axonal changes [2], while descriptions from Alaskan Malamutes are differing [3, 4]. However, in-depth studies of nerves from affected Alaskan Malamute dogs have not previously been performed.

Naturally occurring neuropathies in dogs are increasingly recognized as models for human neuropathies [24,25]. As opposed to experimental rodents, dogs naturally develop similar diseases to humans. Dogs also have a larger body size and a life-expectancy that is more comparable to this species. Furthermore, dogs share environmental conditions and lifestyle with humans. Together this makes them excellent translational disease models [2]. The fact that dogs can be investigated with sophisticated standardized neurological and electrophysiological tests is a further advantage, as it allows for a detailed characterization of the disease phenotype .

Table 1
Overview of Alaskan Malamute dogs included in the study.

Case number and sex	Age (years) at sampling	Control number and sex	Age (years) at sampling
1 Female	6	1 Female	8
2 Male	8	2 Female	11
3 Female	3, 4, 9	3 Male	12
4 Female	2, 6**	4 Male	7
5 Female	1, 3	5 Male*	13
6 Male	2		
7 Female	1		
8 Female	1		
9 Female	2		
10 Male*	5		
11 Male*	2		
12 Male	1		
13 Male	6		
14 Female	6		

* All dogs were genotyped except case 10, case 11 and control 5, due to technical problems with DNA extraction from paraffin-embedded material.
** Only muscle biopsies.
Note: All cases except case 1 and 2 were included in [5]. Furthermore, case 3, 5 and 6 were included in [3].

The aim of this study was to describe in detail the morphology of AMP nerves and discuss these changes in relation to the cell biology of NDRG1 and the overall clinical presentation. Furthermore, studying Alaskan Malamutes with a *NDRG1* mutation is relevant to understand more about the involvement of NDRG1 in human diseases.

2. Materials and methods

2.1. Animals

Nineteen privately owned pure-bred Alaskan Malamute dogs (14 affected dogs and 5 controls free from clinical signs of polyneuropathy) were included in the study (Table 1, detailed information in Suppl. Table A.1. Number of dogs analyzed with the methods and age of depicted animals are also provided in the figure legends). Sixteen out of nineteen were genotyped for the *NDRG1*-allele using the previously described TaqMan assay [3]; Twelve dogs ($n=12$) were classified as homozygous mutants (mut/mut) and four dogs were homozygous wild type (wt/wt) ($n=4$). Whether genotyped or not, all affected dogs ($n=14$) were closely related to each other and presented with neurological signs classically associated with AMP. All samples for the study were collected by veterinarians after written consent from the dog owners. No ethics committee approval was required as all samples were taken as part of the standard diagnostic procedures, in vivo ($n=7$) and/or postmortem ($n=15$), and the investigation did not interfere or impede other tests. Information regarding sex, age at sampling, results from electrodiagnostic testing (electromyography (EMG) and motor nerve conduction velocity (MNCV)), and clinical course was collected from the medical records.

2.2. Tissue sampling

Biopsies from the common fibular nerve and the cranial tibial, biceps femoris and gastrocnemius muscles were taken under general anesthesia as part of the diagnostic workup. Formalin-fixed and fresh samples from both nerve and muscles were shipped by courier to diagnostic laboratories for evaluation. Fixed nerve biopsies were resin-embedded and evaluated in semithin sections (1 µm), while fixed muscle biopsies were paraffin-embedded and routinely stained with hematoxylin and eosin. Unfixed biopsies were transported on cold packs and evaluated cryohistologically with a standard panel of histochemical stains and reactions [26].

Postmortem examinations were carried out shortly after pentobarbital-euthanasia. Samples for immunohistochemistry and immunofluorescence were fixed in 10% buffered formalin and subsequently paraffin-embedded. Samples for Western blotting and RT-qPCR were snap frozen in isopentane, transferred to liquid nitrogen and stored at −80 °C until analysis. Samples for electron microscopy and nerve fiber teasing were gently separated into individual fascicles and fixed in 2.5% glutaraldehyde in Sorensen's phosphate buffer (0.1 M, pH 7.4) for 4 h at room temperature. For details about sampled nerves from individual dogs see Suppl. Table A.1. In addition, a routine postmortem examination was performed, including sampling from cranial tibial, biceps femoris and gastrocnemius muscles.

2.3. Western blotting

Nerve samples from four *NDRG1*$^{mut/mut}$ and four *NDRG1*$^{wt/wt}$ Alaskan Malamutes were thawed, and the epineurial fat removed. Western blotting was performed as previously described [7]. Protein transfer efficiency and protein loading were assessed by staining total protein on the PVDF membranes by SYPRO® Ruby Protein Blot Stain (Molecular Probes, Thermo Fisher Scientific). Band signals were quantified with ImageQuant TL (GE Healthcare) and statistical analyses performed with a non-parametric test (Mann Whitney U-test) in GraphPad Prism (GraphPad Software, San Diego, California, USA).

2.4. RT-qPCR

Nerve tissue from four *NDRG1*$^{mut/mut}$ and four *NDRG1*$^{wt/wt}$ Alaskan Malamutes was homogenized in Trizol (Thermo Fisher Scientific) using a Mixer mill 301 (Retsch, Haan, Germany). Following the Trizol extraction, total RNA was further purified with Rneasy Plus minikit (Qiagen). cDNA was synthesized using SuperScript III Reverse Transcriptase, RNase Out, dNTP mix and Random Primers (all from Invitrogen, Thermo Fisher Scientific). qPCR was performed with LightCycler 480 Sybr Green I Master mix (Roche) and cDNA corresponding to 2.5 ng RNA. The following primers were used: caNDRG1-F2 (TGAACAACCCCGAGATGGTG), caNDRG1-R2 (CCCGG AGATCTTGGATGCAG), caGAPDH-1F (GTATGATTCTA CCCACGGCAAAT) and caGAPDH-1R (GATGGACTTCCC GTTGATGACAA). Samples were run in quadruplets in a total volume of 20 µl. The LightCycler 96 System (Roche) was run under the following conditions; 5 min at 95 °C, 40 cycles of 10 s at 95 °C, 10 s at 60 °C, and then 10 s at 72 °C; and melting curve with 5 s at 95 °C, 1 min at 65 °C and 97 °C.

Statistics (Mann Whitney U-test) were performed in GraphPad Prism.

2.5. Processing for transmission electron microscopy and nerve fiber teasing

Processing for transmission electron microscopy and nerve fiber teasing were performed as previously described [27].

2.6. Antibodies

Details about the antibodies used in the different analyses are specified in Table 2.

2.7. Immunofluorescence and immunohistochemistry

Sections of 3–4 µm from formalin-fixed and paraffin-embedded tissues were placed on glass slides (Superfrost Plus®, Menzel Gläser, Thermo Fisher Scientific) and stored at 4 °C until staining. Previously described protocols were used for immunofluorescence [7] and immunohistochemistry [27].

2.8. Morphometry

Images from semithin sections of n. fibularis communis ($n = 8$) or n. tibialis ($n = 3$) were evaluated by Image-Pro Plus (Media Cybernetics, Rockville, Maryland, USA). The area of the nerve fibers and axons were measured. Thereafter, the diameters of these were derived from the area of a circle of equivalent area [28], and the g-ratios calculated. Statistics (Mann Whitney U-test) were performed in GraphPad Prism. An example of the image analysis is provided in Supplementary Fig 1.

2.9. Extraction and analysis of lipids from peripheral nerves

Lipid extraction from nerves and non-targeted lipid analysis were performed as previously described [27]. Briefly, snap frozen nerve tissue (50 mg) was homogenized with a bead homogenizer and lipids were extracted using mixture of chloroform and methanol. The lipid analysis was carried out using the supercritical fluid chromatographic system Acquity UPC2® coupled to a quadrupole time-of-flight mass spectrometer SYNAPT G2-S HDMS (both Waters, Milford, Massachusetts, USA). The method used allows detection of TG, DG, MG, Cer, HexCer, HexCer(OH), SM, FC, CE, PG, PC, LPC, PE and LPE. Non-targeted data were processed with Progenesis QI enabling export of list of compounds found along with their abundances. Data were further filtered using an in-house developed script collecting total abundances for

Table 2
Antibodies and dilutions used in the analyses.

Name	Catalog number	Producer	Dilutions		
			IF	IHC	WB
Anti-NDRG1	WH0010397	Sigma-Aldrich, Merck, Darmstadt, Germany	1/2000	NA	1/2000
Phospho-specific anti-NDRG1 (Thr346)	5482	Cell Signaling Technology, Leiden, Netherlands	NA	NA	1/1000
Anti-neurofilament 200	064H-4809 (batch number)	Sigma-Aldrich, Merck, Darmstadt, Germany	1/400	NA	NA
Anti-beta actin	MA1–140	Invitrogen, Thermo Fisher Scientific, Massachusetts, USA	1/2000	NA	NA
Anti-CD3	A-0452	Dako, California, USA	NA	1/500	NA
Anti-CD79	NB100–64,347	Novus Biologicals, Colorado, USA	NA	1/750	NA
Anti-Iba1	019–19,741	Fujifilm Wako Chemicals, Neuss, Germany	NA	1/250	NA

IF = Immunofluorescence, IHC = Immunohistochemistry, WB = Western blotting, NA = Not analyzed.

each individual lipid class. Response factors (Rf) were used for correction of raw abundances to show semi-quantitative composition of lipid classes in the studied samples. Rf were determined experimentally by comparing abundances of lipid standards, one representative per each class, of equal concentration. Two-tailed independent *t*-test was performed to evaluate statistical difference in lipid class distribution between the groups.

3. Results

3.1. Long-term clinical course and electrodiagnostic examination

Four of the 14 affected dogs were euthanized, at the owner's request, in conjunction with the diagnosis of AMP. Ten of the affected dogs were allowed to survive this disease stage and followed up (median 44 months, range 12–100 months) by repeated examinations or contact with clinicians in the research group. In three of these 10 dogs, the clinical signs gradually progressed until euthanasia. In one other dog, the clinical signs progressed in the two years following diagnosis, but the dog was subsequently lost to follow up. In the remaining six dogs followed up, both the gait abnormalities and the exercise intolerance slowly improved during the months after nadir and then stabilized. However, none of the dogs returned to normal and the inspiratory stridor persisted. At a later stage (at the age of 3 and 6 years, respectively), two affected dogs presented with regurgitation due to development of megaoesophagus (Suppl. Fig. 2) and were then euthanized. Eleven of the 14 affected dogs were subjected to postmortem examination and autopsy confirmed megaoesophagus in three dogs (including the two dogs with regurgitation).

MNCV in the fibular ($n = 4$, mean 23.13 m/s, SD 14.24, reference 79.8±1.9 [29]) and ulnar nerves ($n = 10$, mean 37.5 m/s, SD 12.73, reference 58.9±1 [29]) were decreased in all the examined dogs (Suppl. Table 1). In two dogs, MNCV could not be determined as no compound muscle action potential (CMAP) was produced by stimulation. EMG revealed spontaneous activity in several muscles in all dogs tested ($n = 10$). In two dogs, repeated MNCV measurements were performed. For case three, the MNCV in the ulnar nerve was 30, 40 and 56.3 m/s at the age of three, eight and nine years, respectively. Furthermore, the MNCV in the fibular nerve was 31.4 m/s at the age of three years, but not possible to measure at the age of nine. For case four, the MNCV in the fibular nerve was 29 m/s and 26.9 m/s at the age of two and five years, respectively.

3.2. Levels of NDRG1 protein and mRNA

Nerves from affected dogs had reduced NDRG1 protein levels compared to controls (Figs. 1A, C). The intensity of the 42 kDa band, corresponding to the full length protein, as well as the bands with molecular weights between 32 and 40 kDa, were reduced by approximately 70% in the *NDRG1*$^{mut/mut}$ dogs ($p = 0.029$). Additionally, there was a significant reduction in signal intensity from the band corresponding to NDRG1 phosphorylated at residue Thr346 (pNDRG1) in this group of dogs ($p = 0.029$, Figs. 1B, C). In contrast, the mRNA levels in nerves of *NDRG1*$^{mut/mut}$ dogs normalized to *GAPDH* were not significantly different from the controls ($p = 0.2$, Fig. 1D). It should be noted that *GAPDH* has not been validated as a reference gene for mRNA expression analysis in nerves of dogs, thus the result should be interpreted with caution.

3.3. Pathology

3.3.1. Teased nerve fibers

In nerves from affected dogs examined by nerve fiber teasing, internodal lengths and myelin thickness varied (Fig. 2). Demyelinated segments and short internodes with reduced myelin thickness (intercalated internodes), consistent with remyelination, were present. The changes had a multifocal distribution, and severely affected internodes intermingled with internodes without observable changes. This distribution is typical for a demyelinating disease [30,31]. In some cases, paranodal retraction and widening of the nodal gap were evident. Focal thickenings of the nerve fibers were present, mostly internodally, occasionally

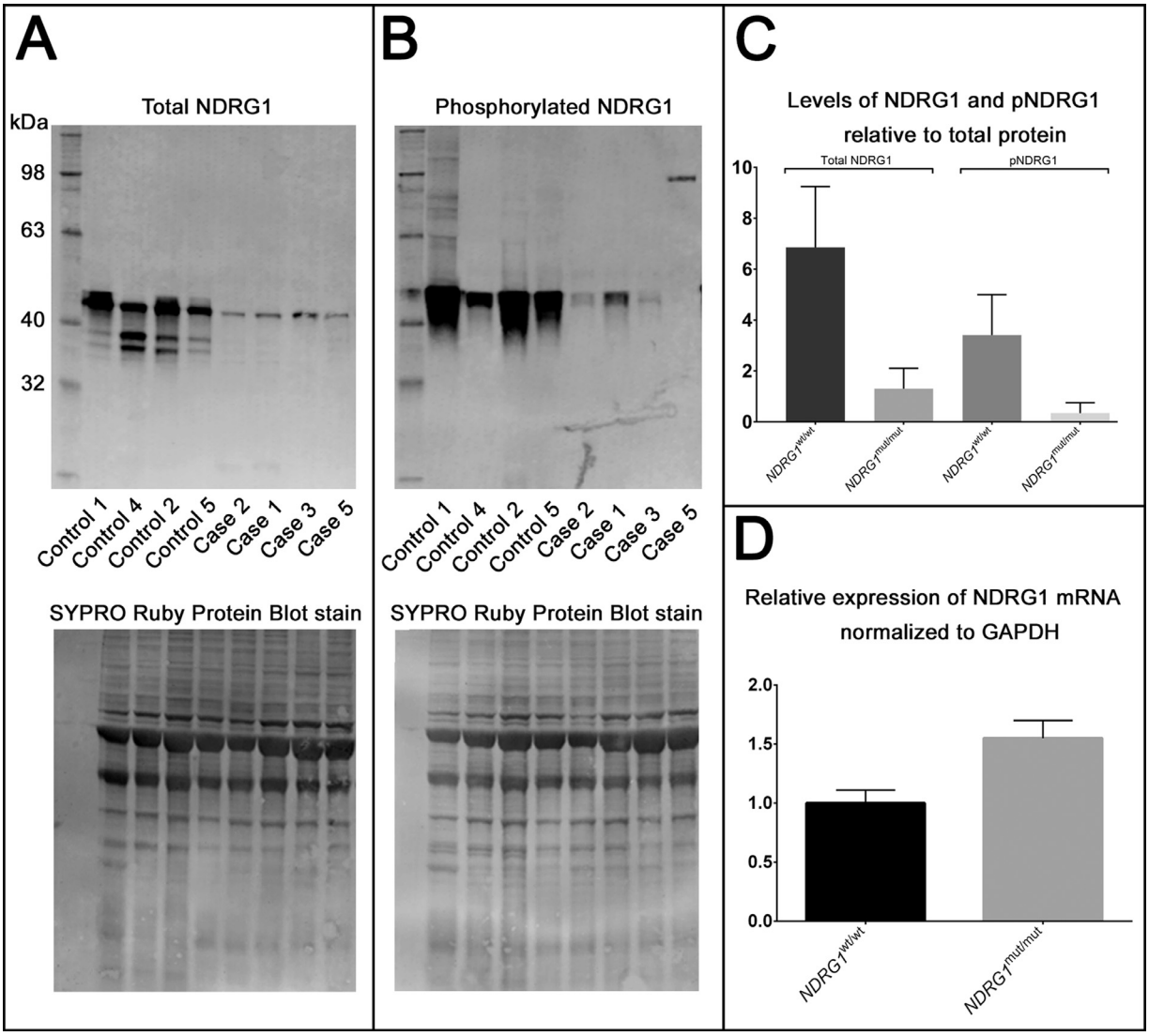

Fig. 1. **A, B.** Western blot of nerve lysate from Alaskan Malamute controls ($n=4$) and cases ($n=4$) with antibodies against NDRG1 (**A**) and phospho-NDRG1 (**B**). **C.** Semiquantification of NDRG1 protein in nerve lysates based on band intensity in Western blot (mean+SD). There is a significant reduction in the levels of both total NDRG1 ($p=0.029$) and pNDRG1 ($p=0.029$) in NDRG1$^{mut/mut}$ Alaskan Malamutes compared to controls. **D.** Relative expression of NDRG1 mRNA in nerve samples (mean+SD) from Alaskan Malamutes controls ($n=4$) and cases ($n=4$). Relative expression levels were calculated using the Relative Standard Curve method with standard curves obtained from a random sample, and *NDRG1* expression was normalized to *GAPDH*. The difference between the groups was not significant ($p=0.2$).

close to the Schwann cell perikaryon (Fig. 2d), but paranodal localization was also observed. At this level, it was not possible to ascertain whether the swellings derived from the axon, the Schwann cell or both. Wallerian-like axonal degeneration was observed in only a few fibers (not shown).

3.3.2. Light microscopy

Nerves from *NDRG1*$^{mut/mut}$ Alaskan Malamutes exhibited a loss of large myelinated fibers (Fig. 3A) accompanied by a concurrent increase in endoneurial connective tissue. These changes varied inter- and intraindividually from only mild affection to severe loss of fibers with concomitant fibrosis. As shown morphometrically for the common fibular nerve, there was a shift in the distribution of myelinated nerve fibers towards smaller diameter fibers (Fig. 3B). As the same shift was observed in axonal diameter-frequency histograms, this shift is probably caused by a combination of loss of large myelinated fibers and reduced myelin thickness. While the fibular nerves from the *NDRG1*$^{wt/wt}$ Alaskan Malamutes had the expected bimodal diameter distribution of myelinated fibers [32], the distribution in nerves from some of the cases approached unimodality (for example case four). For case three and five, biopsies taken at different ages allowed assessment of a potential disease progression. The investigations showed a shift towards thinner fibers at greater age. The myelinated fiber density was not significantly different between the groups ($p=0.1429$. Controls: $n=2$, mean: 4798.2 MF per mm^2, SD 959.2. Cases: $n=6$, mean: 6058.9 MF per mm^2, SD 1021.4).

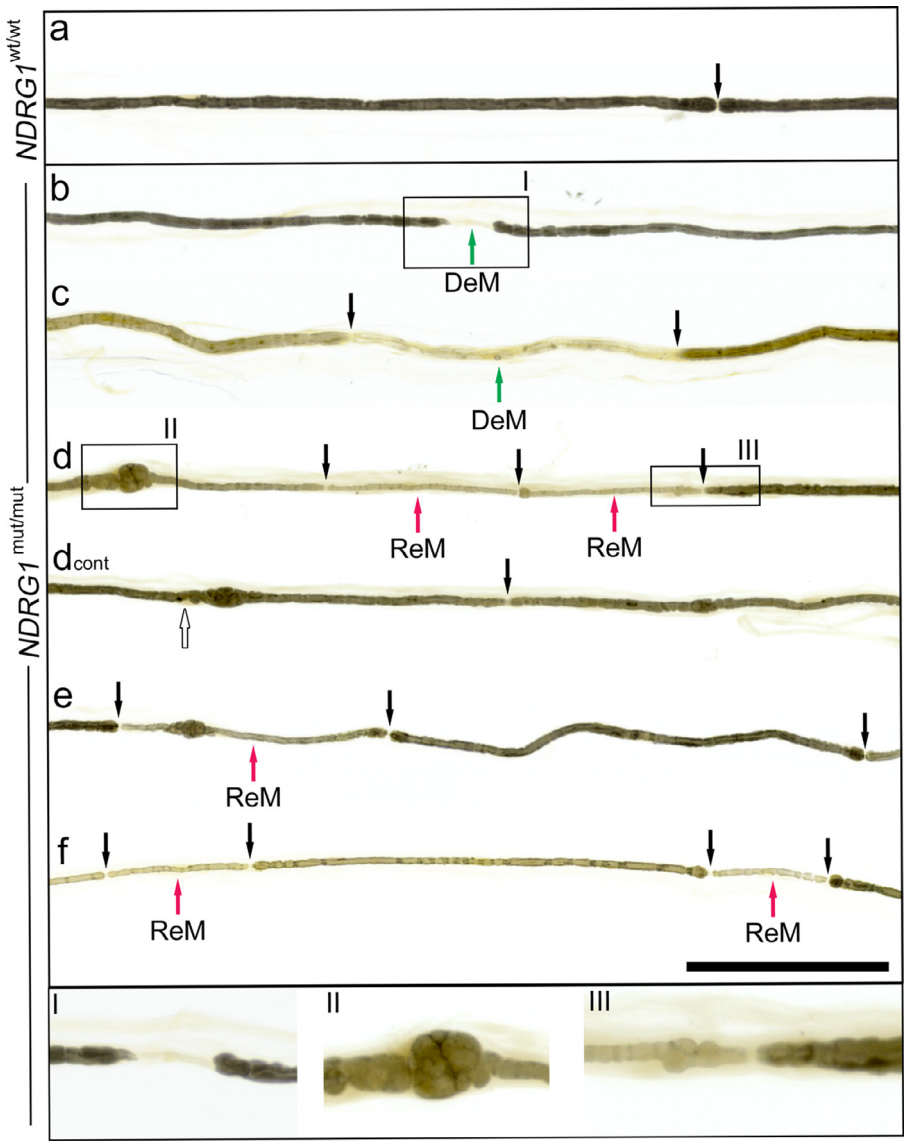

Fig. 2. Teased nerve fibers, representative examples from controls (**a**, $n=2$) and cases (**b-f**, $n=4$). Boxes indicated by roman numerals are magnified in the lower part of the figure. In fibers from cases, paranodal (**b**, magnified in **I**) and segmental demyelination (**c**) were present. Focal thickenings of the nerve fiber were observed internodally (**d**, **e**, magnified in **II**), occasionally close to the Schwann cell nucleus (**d**, white arrow). Short and thinly myelinated internodes, consistent with remyelination, intermingled with longer internodes with thicker myelin sheath (**d-f**, magnified in **III**). Nodes of Ranvier are indicated by black arrows. DeM = Demyelinated segment. ReM = Remyelinated segment. Bar 200 μm. Origin of depicted fibers and age at sampling: Control 2 (11 years old, **a**), case 1 (6 yo, **b**, **d**, **e**), case 2 (8 yo, **f**), case 3 (9 yo, **c**).

When nerves were studied at higher magnification, many of the remaining fibers had thin myelin sheaths in relation to the axonal size (Figs. 4E-G), in agreement with results from the study of teased fibers and our finding that the g-ratios of the *NDRG1*$^{mut/mut}$ Alaskan Malamutes were shifted towards higher values compared to the control (Suppl. Fig. 3). Presumptive regenerative clusters were observed in some of the nerves (Fig. 4E). Swollen nerve fibers were present in the nerves from the *NDRG1*$^{mut/mut}$ Alaskan Malamutes (Figs. 4F, G) and studied more closely at the ultrastructural level (see Section 3.3.3).

Lesions were observed in both proximal (for example nerve roots and sciatic nerves) and distal nerve segments (such as tibial, fibular and recurrent laryngeal nerves), long (for example recurrent laryngeal nerve) and short nerves (obturator nerve), and involved both mixed and purely sensory nerves (superficial radial nerve).

In skeletal muscle, angular atrophy of myofibers (varying from scattered singular to small and large groups) were present (Fig. 4A), in accordance with denervation atrophy following axonal loss. The angular atrophied fibers were of both fiber types as shown by the ATPase reaction (Fig. 4B). The normal mosaic pattern of muscle fiber types was regionally absent in some cases with fiber type grouping, supporting attempts at reinnervation (Fig. 4B).

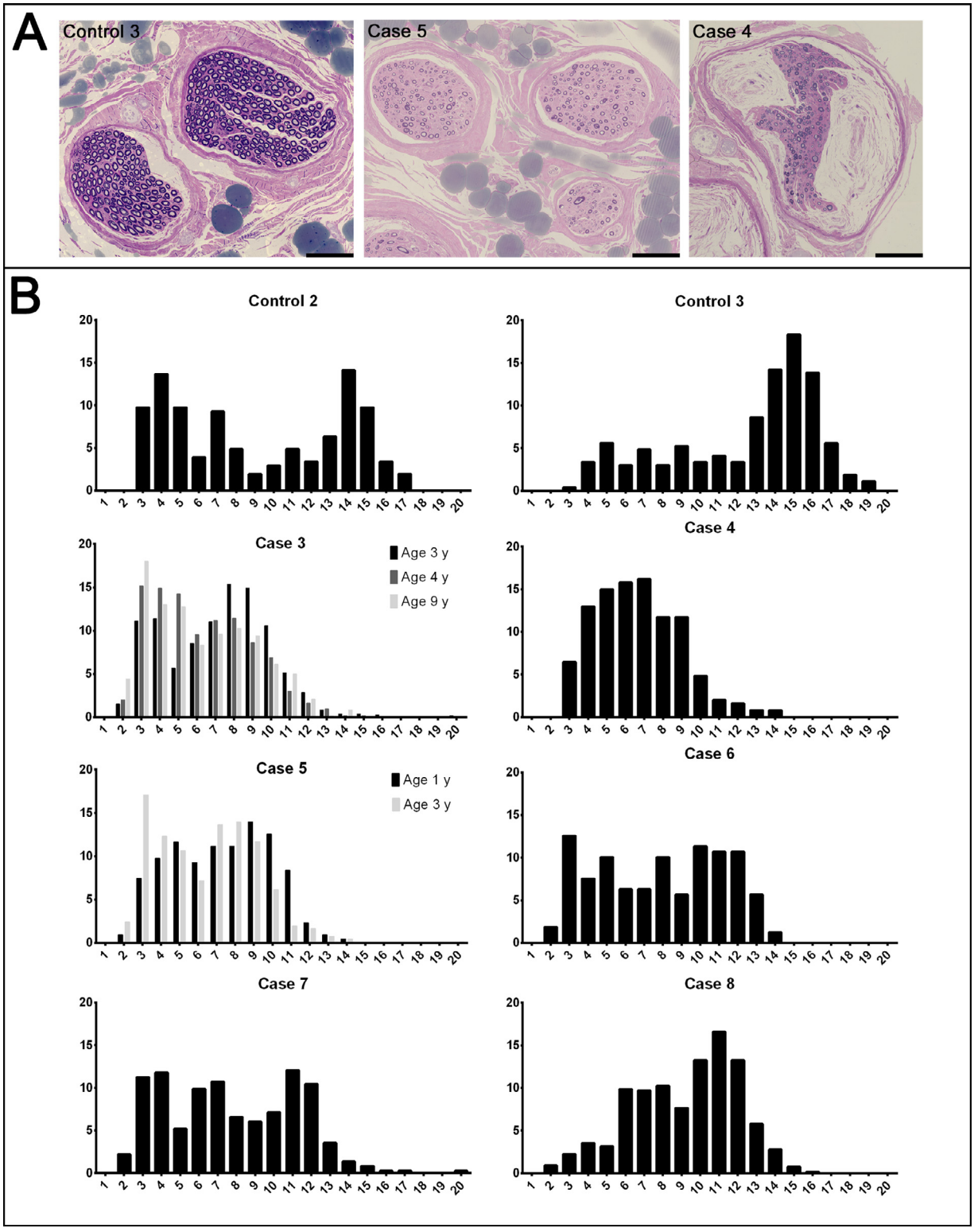

Fig. 3. Semithin sections (A) and myelinated fiber diameter-frequency histograms (B) from the common fibular nerve of controls ($n=2$) and cases ($n=6$). **A**. Note the reduction of large myelinated fibres in the cases. The prominent Renaut bodies observed in case 4 are not typical findings in affected dogs. Bar 100 μm. **B**. There is a shift in the distribution of myelinated fibres in the cases. For case 3 and 5, morphometrical comparison of biopsies taken at different ages is included in the histogram. *Y*-axis: Percentage of myelinated fibers. *X*-axis: Diameter of myelinated fibers in μm. Age at sampling: Control 2 (11 years old), control 3 (12 yo), case 3 (3, 4, 9 yo), case 4 (2 yo), case 5 (1, 3 yo), case 6 (2 yo), case 7 (1 yo), case 8 (1 yo).

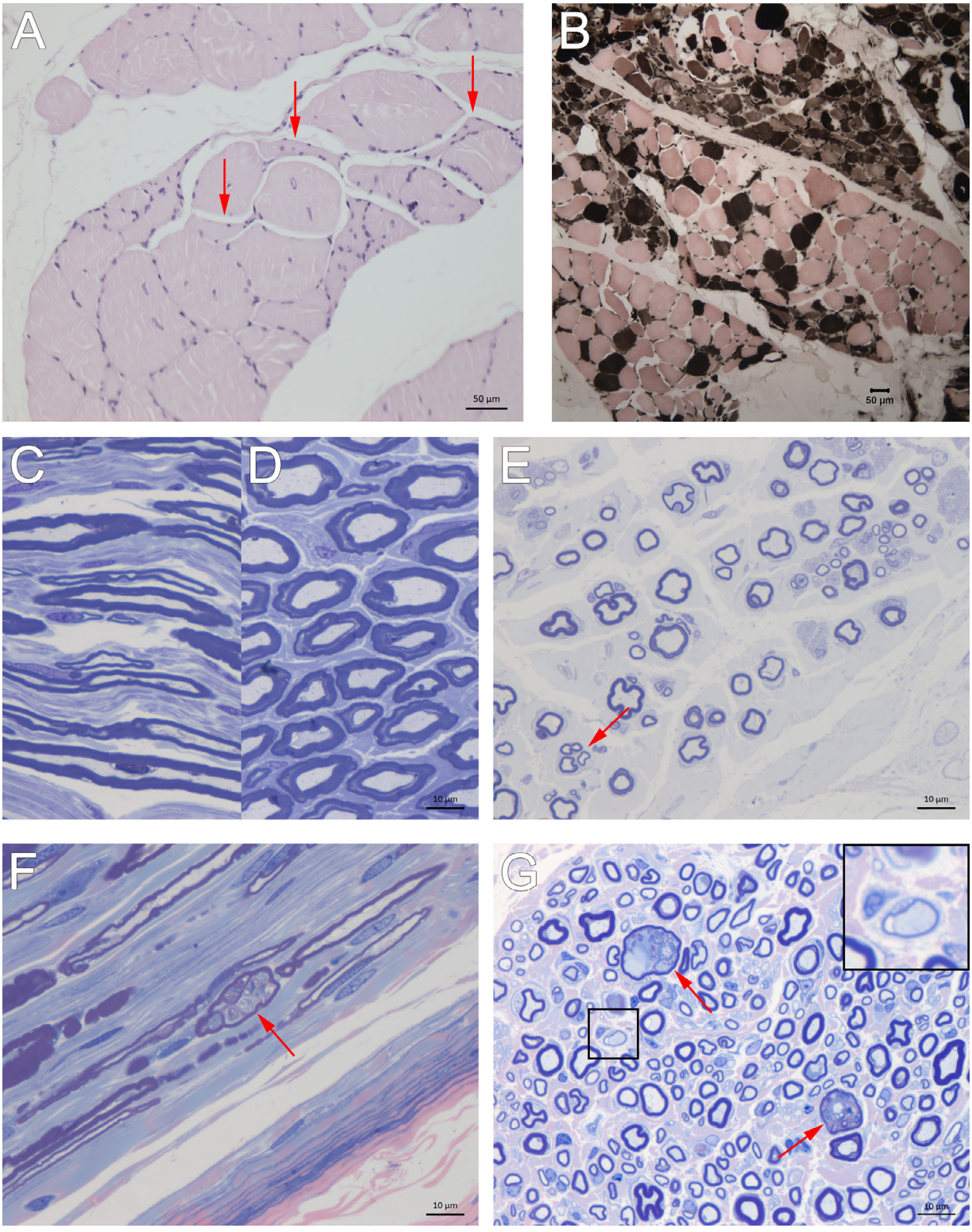

Fig. 4. Representative light micrographs of skeletal muscle (**A, B**) and nerves (**C–G**) from affected (**A, B, E–G**, $n=8$) and control (**C, D**, $n=3$) Alaskan Malamutes. **A**. Scattered and small groups of angular, atrophic myofibers (arrows) in the gastrocnemius muscle (case 3, 9 years old). **B**. Fiber type grouping in the gastrocnemius muscle (case 5, 1 yo). Type 1 muscle fibers are dark, while type 2 are pale. **C, D**. Nerve from a control Alaskan Malamute (control 1, 6 yo). **E**. Axonal loss and thinly myelinated (remyelinating) fibers in nerve from affected Alaskan Malamute (case 2, 8 yo). A presumptive regenerative fiber cluster is indicated by red arrow. **F, G**. Focal swelling of nerve fibers (red arrows) is seen in both longitudinal (**F**) and transverse (**G**) sections (case 1, 6 yo). A myelinated fiber with very thin myelin sheath is highlighted (box and inset) in **G**. Stained with hematoxylin and eosin (**A**), Myofibrillar ATPase reaction at pH 4.3 (**B**), toluidine (**C–E**), toluidine and safranin-O (**F, G**).

3.3.3. Ultrastructural pathology

The ultrastructural examination confirmed the presence of thinly myelinated nerve fibers and small onion bulbs (not shown). Onion bulbs and thinly myelinated nerve fibers suggest repeated episodes of demyelination and remyelination. Macrophages with intracytoplasmic vacuoles were present around demyelinated nerve fibers and also observed intratubary (not shown). The presence of Iba1+-macrophages in the endoneurium was confirmed by immunohistochemistry (see Section 3.3.5).

A frequent finding was accumulation of filamentous material in the cytoplasm of myelinating Schwann cells. This material was observed in the adaxonal Schwann cell cytoplasm or in the inner part of dilated Schmidt-Lanterman clefts (Figs. 5A). Occasionally, the Schmidt-Lanterman clefts were disrupted and then associated with dyscompacted myelin sheaths mixed with a pleomorphic, coarsely granular osmiophilic material (Figs. 5B, C) dispersed between the sheets. This morphologically heterogenous material probably consists of a mixture of the aforementioned filamentous material and lipids from myelin degradation as it intermingled with fragments of periodically structured lamellae [33].

Focally folded myelin was often observed consisting of infoldings derived from the inner part of the myelin sheaths (Figs. 5D, E, F). The folds evolved from the Schmidt-Lanterman clefts (Fig. 5D) and occasionally seemed to subdivide the axon into pockets (Fig. 5E, F). This resulted in several axonal structures enclosed by the same myelin sheath, separated by thin myelin septa derived from the adaxonal part of the sheath (Figs. 5B, D–F). Degenerating organelles were present in the myelin-enclosed axonal pockets (Figs. 5B, D–F), suggestive of disrupted axonal transport and early axonal degeneration. Despite an overall increase in nerve fiber diameter, the diameter of the axon was often reduced and the axonal outline distorted in the segments with focally folded myelin, seemingly compressed by the myelin infoldings and adaxonal Schwann cell material (Figs. 5B, E). Artefactual changes can be produced by delayed fixation, however, as the ultrastructural changes reported were also present in nerve biopsies fixed immediately after surgical removal, we consider it unlikely that the reported changes are artefacts.

3.3.4. Immunofluorescence

As structures resembling Hirano bodies, containing actin and actin-related proteins [34], have been described in the Schwann cell cytoplasm of rodents with *Ndrg1* mutations [9], immunofluorescence was performed with antibodies against β-actin and neurofilament. In nerves from the *NDRG1*$^{mut/mut}$ Alaskan Malamutes, β-actin-positive aggregates were present multifocally in myelinating Schwann cells (Fig. 6, Suppl. Fig. 4). More specifically, the β-actin signal was present in thin strands and occasionally formed circular or semi-circular structures. The diameter of the neurofilament-positive axon was reduced in these areas, but axonal swellings were present in adjacent segments. Occasionally, the actin-positive material surrounded small axonal structures only coupled to the main axonal structure through thin connections.

Table 3
Relative lipid class distribution in peripheral nerves from Alaskan Malamute polyneuropathy cases (*NDRG1*$^{mut/mut}$) and controls (*NDRG1*$^{wt/wt}$).

Lipid class	*NDRG1*$^{wt/wt}$ ($n=3$)		*NDRG1*$^{mut/mut}$ ($n=3$)		*t*-test
	Mean%	SD	Mean%	SD	*P*-value
MG	0.79	0.5	0.88	0.8	0.83521
DG	2.29	0.7	1.97	1.1	0.63792
TG	55.31	11.5	78.01	12.4	0.06677
HexCer	3.70	1.3	0.99	0.5	0.03254
HexCer(OH)	1.33	0.4	0.37	0.2	0.02726
CE	2.85	1.6	5.53	4.8	0.29980
PC	6.31	1.5	3.30	1.4	0.06620
FC	0.20	0.1	0.09	0.1	0.07106
SM	21.73	4.8	5.99	3.0	0.00943
LPC	0.05	0.0	0.06	0.0	0.68876
PE	5.43	1.7	2.81	1.7	0.10401

MG = Monoacylglycerols, DG = Diacylglycerols, TG = Triacylglycerols, HexCer = Hexosylceramides, CE = Cholesteryl esters, PC = Phosphatidylcholines, FC = Free Cholesterol, SM = Sphingomyelins, LPC = Lysophosphatidylcholines, PE = Phosphatidylethanolamines.

3.3.5. Immunohistochemistry

Infiltration and/or proliferation of macrophages, T- and B-lymphocytes in the nerves were investigated with antibodies against Iba1, CD3 and CD79, respectively. While increased numbers of Iba1+ cells in the endoneurium were observed in *NDRG1*$^{mut/mut}$ Alaskan Malamutes compared to *NDRG1*$^{wt/wt}$, no difference between the genotypes was observed for CD3 and CD79 (not shown).

3.4. Lipid analysis

Analysis of peripheral nerve lipid composition revealed significant decreases in hexosylceramides (HexCer) and sphingomyelins (SM) in the relative lipid class distribution in the *NDRG1*$^{mut/mut}$ Alaskan Malamutes compared to *NDRG1*$^{wt/wt}$ (Suppl. Fig. 5 and Table 3).

4. Discussion

Neuropathies can be caused by malfunctions at either end of the axo-glial communication axis; i.e., be primary axonal or primary glial cell disorders. This distinction is important for understanding the etiology and molecular pathology of a given disease, but can be difficult to ascertain due to overlapping clinical and pathological features, regardless of the primary defect [35–37]. Since NDRG1 is expressed in Schwann cells and not axons, polyneuropathies associated with mutations in *NDRG1* are expected to result from compromised Schwann cell functions. In accordance with this, human CMT4D patients show demyelinating changes in childhood, rapidly followed by axonal loss [9,38] and severe clinical signs [38,39]. In mice models of this disease, demyelination is the dominant feature, with less pronounced axonal loss [9]. In this report, we provide a detailed characterization of the *NDRG1*-associated Alaskan Malamute polyneuropathy, revealing previously unrecognized features.

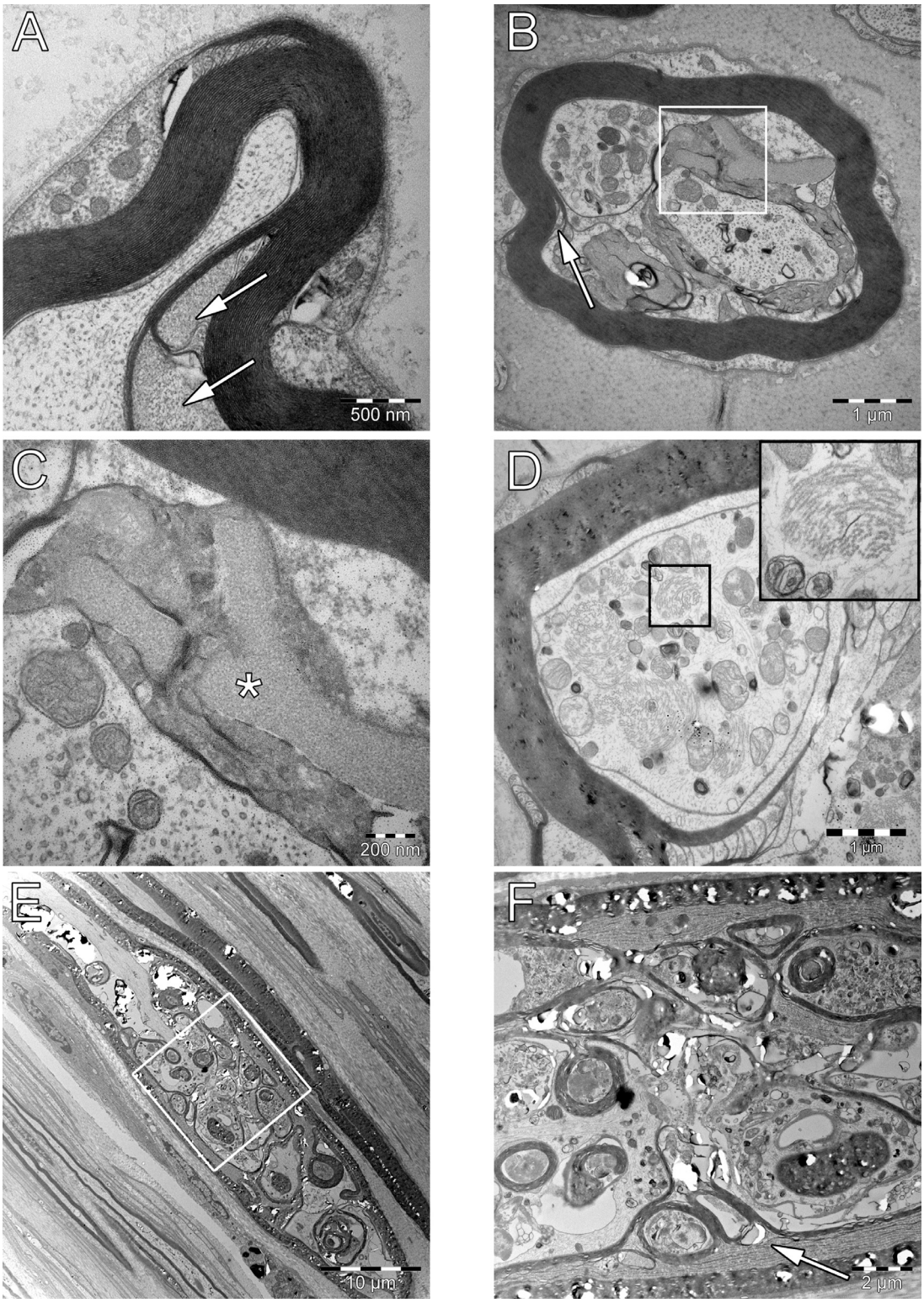

Fig. 5. Electron micrographs of nerves from affected Alaskan Malamutes ($n = 8$), transverse **(A-D)** and longitudinal **(E, F)** sections. **A**. Accumulation of filamentous material in the inner part of distended Schmidt-Lanterman clefts. **B, C.** Disrupted Schmidt-Lanterman cleft (arrow in **B,** white box magnified in **C**) with coarsely granular material (asterisk in **C**) between dyscompacted myelin lamellae from the inner part of the myelin sheath. Note the two axonal structures within the myelin sheath in **B**, both with aggregates of mitochondria. **D, E, F.** Infoldings of the myelin sheath, originating from a Schmidt-Lanterman cleft (**D**), seemingly dividing the axon into several structures. The axonal cytoplasm contains accumulated organelles, including degenerating mitochondria (**D-F**) and aggregates of neurofilaments (black frame in **D**, magnified in inset), consistent with early axonal degeneration. The focal distribution of changes are shown in **E** (white frame magnified in **F**). Arrow (**F**) indicate dyscompacted myelin. Origin of electron micrographs and age at sampling: Case 1 (6 years old, **A**), case 3 (9 yo, **B**, **C**, **E**, **F**), case 2 (8 yo, **D**).

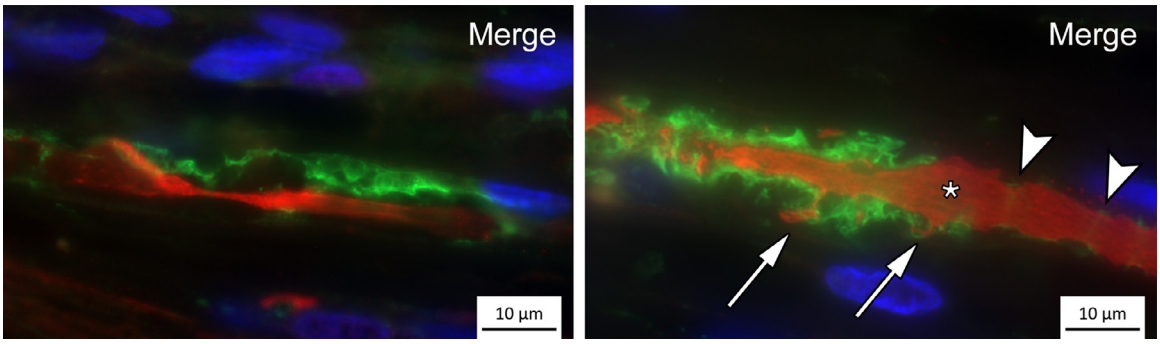

Fig. 6. Immunofluorescence on nerve sections (cases $n=3$, controls $n=2$). Representative images from case 5 (3 years old) with antibodies against beta-actin (green) and neurofilament (red), two different nerve fibers are shown. Nuclei are stained with DAPI (blue). Aggregates of actin are present in the nerves of affected Alaskan Malamutes. Note the difference between the aggregates and the sparse amount of actin normally present in the Schmidt-Lanterman clefts (arrowheads). Although the axonal diameter was reduced in the areas with aggregates, the axon was swollen adjacent to these segments (asterisk). Note the small axonal structures within the actin-positive areas only coupled to the main axon through thin connections (arrows).

The changes observed in the nerves of affected Alaskan Malamutes in this study indicate a demyelinating disease with remyelination, characteristic axonal changes and eventually loss. Thus, Alaskan Malamutes with *NDRG1* mutations are apparently more similar to humans with CMT4D than the rodent models where axonal involvement is milder [9,23,39,40]. Our findings contrast with previous reports from dogs [2, 3]. In a study of Greyhounds lacking NDRG1 [2], and in a previous report on the same AMP as presented here [3], it was concluded that the disease was predominantly axonal or mixed due to the presence of degenerative axonal changes in segments without concurrent myelin abnormalities. In the Greyhounds, thinly myelinated (i.e. remyelinated) nerve fibers, dyscompaction of the adaxonal myelin sheath and granulofilamentous inclusions in the Schwann cell cytoplasm were also observed [2]. Thus, the changes in nerves of humans, rodents and dogs with NDRG1 abnormalities share certain similarities, and AMP is indeed a new model for human CMT4D, replicating both the demyelination and axonal changes, in both motor and sensory nerve fibers, present in the human disease [23,40].

A progressive polyneuropathy is described in human CMT4D patients with gait disturbance in their first decade, upper limb involvement in their second and sensorineural deafness in their third decade of life [38]. Disease progression in affected Alaskan Malamutes was documented with the diameter shift observed in morphometric analyses of semi-thin nerve sections from a few dogs. Results from electrodiagnostic examinations were in agreement with a polyneuropathy involving motor nerve fibers, but in Case 3, serial measurements revealed improved MNCV with increasing age - in accordance with her clinical development during adulthood. The observed increase in MNCV is in accordance with remyelination of previously demyelinated internodes, through which the nerve conduction velocity might recover to at least 60% of normal [41]. The remyelinated internodes remain thinner than normal, explaining the reduction in myelinated fiber diameter observed by morphometry in the same dog.

The filamentous material present in the adaxonal cytoplasm and inner part of the Schmidt-Lanterman cleft resembles inclusion material reported from the same location in nerves of human CMT4D patients and rodent models of this disease [9,23,39,40]. In humans with CMT, this material is seemingly specific for the 4D subtype [40,42], however, to the best of our knowledge, the content of the material has not been ascertained. From studies in rodents, the inclusions have been proposed to represent Hirano bodies based on morphological criteria [9], but in human CMT4D nerves, a similar material did not have the structured morphology of true Hirano bodies [23]. Hirano bodies are described as paracrystalline inclusions consisting of sheets of parallel actin filaments [34]. The filamentous material observed in the nerves of affected Alaskan Malamutes lacked the paracrystalline structure reported from rodents [9,43], but otherwise resembles the inclusion material reported from humans and rodents by its ultrastructural morphology and localization. Furthermore, we confirm its richness in actin by immunofluorescence.

Actin polymerization occurs in Schwann cells in both health and disease. Actin remodelling drives the membrane extension during normal myelination [44] as well as in conditions with excessive myelin growth [45]. Furthermore, actin polymerization occurs in Schmidt-Lanterman clefts during Wallerian degeneration [46], and recently, signaling from injured axons were shown to trigger formation of constricting actin spheres in Schwann cells, important for swift removal of the degenerating axon [47]. Actin polymerization was also found in the Schmidt-Lanterman clefts and adaxonal Schwann cell cytoplasm of Tibetan Mastiffs with Inherited Hypertrophic Neuropathy, where the filaments ultimately caused distension of the Schwann cell cytoplasm and subdivision of the axon [31,48,49], strongly resembling the apparent division of the axon regionally within one myelin sheath observed in the AMP nerves. This change is also described from Greyhounds lacking NDRG1 [2], but not reported in CMT4D [9,23,39,40,50–52]. It remains to investigate the relationship between NDRG1 functions and

actin polymerization in Schwann cells and the possible role of filaments in the intrusion of the Schwann cell into the axon. The intrusions with myelin infoldings could represent focal hypermyelination, caused by reduced NDRG1 activity in Schwann cells, and the actin aggregates observed in the Schmidt-Lanterman clefts of AMP nerves could conceivably be an early stage in the uncontrolled membrane growth ultimately leading to formation of myelin folds [45] and axonal degeneration.

We have previously shown that phosphorylated NDRG1 preferentially localized to the abaxonal cytoplasm and outer aspects of the Schmidt-Lanterman clefts in myelinating Schwann cells of normal dogs by immunofluorescence, while no pNDRG1 signal was observed in an affected Alaskan Malamute [7]. Phosphorylated NDRG1 (Thr346) has been suggested to participate in termination of myelination, as loss of serum glucocorticoid kinase 1 (Sgk1), with less pNDRG1 as a sequel, caused hypermyelination in mice [17]. We did not observe decreased g-ratios in the *NDRG1*$^{mut/mut}$ Alaskan Malamutes, as would be expected in a condition with diffuse hypermyelination. However, in conditions with focal hypermyelination, a reduced g-ratio may not be found [53], as most cross-sections of nerves with focally folded myelin will be represented in a semithin section by a nerve segment with normal myelination. Further studies are needed to investigate whether the *NDRG1* mutation disrupts signalling in the Schwann cells by affecting the phosphorylation of the encoded protein, either directly or indirectly.

Analysis of peripheral nerve lipid composition revealed several differences between the genotype groups. Loss of NDRG1 function can conceivably affect lipid composition of the nerves directly, as NDRG1 participated in vesicular recycling of the low-density lipoprotein receptor (LDLR) in epithelial cells [12] and regulated lipid metabolism in breast cancer cells [16]. In the latter, silencing of NDRG1 resulted in increased triacylglycerol levels. However, unspecific changes caused by loss of myelin and axons in the AMP nerves precludes interpretation of changes specifically related to loss of NDRG1 function. These include for example the observed significant reduction in the levels of sphingomyelins and glycolipids [54]. Thus, a specific contribution to the observed differences in lipid composition from loss of NDRG1 function cannot be ruled out, but needs further investigation.

The Western blots showed that the nerve levels of NDRG1 in the affected Alaskan Malamutes were significantly reduced, but not completely lost. In contrast, Greyhounds with *NDRG1*-associated neuropathy were reported to have a total NDRG1-deficiency [2], just as in humans with CMT4D caused by a nonsense mutation [9]. The incomplete loss of NDRG1 function in the Alaskan malamutes results in a later onset and milder clinical course of AMP as compared with the neuropathies in Greyhounds and the *stretcher* mouse model [9] in which there is complete loss of NDRG1.

In conclusion, Alaskan Malamutes with *NDRG1* mutations is a unique spontaneous model, which demonstrates morphological features resembling the human CMT4D, but also reveals some previously undescribed changes.

Acknowledgments

The authors thank Mari Katharina Aas Ådland for technical assistance. We are also grateful to all dog owners and veterinarians who have contributed with information, and all colleagues that have assisted us in the sampling procedures.

Supplementary materials

Supplementary material associated with this article can be found, in the online version, at doi:10.1016/j.nmd.2020.11.010.

References

[1] Kalaydjieva L, Gresham D, Gooding R, Heather L, Baas F, de Jonge R, et al. N-myc downstream-regulated gene 1 is mutated in hereditary motor and sensory neuropathy-Lom. Am J Hum Genet 2000;67:47–58.
[2] Drogemuller C, Becker D, Kessler B, Kemter E, Tetens J, Jurina K, et al. A deletion in the N-myc downstream regulated gene 1 (NDRG1) gene in Greyhounds with polyneuropathy. PLoS One 2010;5:e11258.
[3] Bruun CS, Jaderlund KH, Berendt M, Jensen KB, Spodsberg EH, Gredal H. A Gly98Val mutation in the N-Myc downstream regulated gene 1 (NDRG1) in Alaskan Malamutes with polyneuropathy. PLoS One 2013;8:e54547.
[4] Moe L. Hereditary polyneuropathy of Alaskan malamutes. In: Kirk R, Bonagura J, editors. Kirks current veterinary therapy. St. Louis, Missouri: Saunders; 1992. p. 1038–9.
[5] Jäderlund KH, Rohdin C, Berendt M, Stigen Ø, Fredholm M, Espenes A, et al. *Re*-emergence of hereditary polyneuropathy in Scandinavian Alaskan malamute dogs—Old enemy or new entity? A case series. Acta Vet Scand 2017;59:26.
[6] Lachat P, Shaw P, Gebhard S, van Belzen N, Chaubert P, Bosman FT. Expression of NDRG1, a differentiation-related gene, in human tissues. Histochem Cell Biol 2002;118:399–408.
[7] Skedsmo FS, Tranulis MA, Espenes A, Prydz K, Matiasek K, Gunnes G, et al. Cell and context-dependent sorting of neuropathy-associated protein NDRG1 – insights from canine tissues and primary Schwann cell cultures. BMC Vet. Res. 2019;15:121.
[8] Berger P, Sirkowski EE, Scherer SS, Suter U. Expression analysis of the N-Myc downstream-regulated gene 1 indicates that myelinating Schwann cells are the primary disease target in hereditary motor and sensory neuropathy-Lom. Neurobiol Dis 2004;17:290–9.
[9] King RH, Chandler D, Lopaticki S, Huang D, Blake J, Muddle JR, et al. Ndrg1 in development and maintenance of the myelin sheath. Neurobiol Dis 2011;42:368–80.
[10] Askautrud HA, Gjernes E, Gunnes G, Sletten M, Ross DT, Borresen-Dale AL, et al. Global gene expression analysis reveals a link between NDRG1 and vesicle transport. PLoS One 2014;9:e87268.
[11] Kachhap SK, Faith D, Qian DZ, Shabbeer S, Galloway NL, Pili R, et al. The N-Myc down regulated Gene1 (NDRG1) Is a Rab4a effector involved in vesicular recycling of E-cadherin. PLoS One 2007;2:e844.
[12] Pietiainen V, Vassilev B, Blom T, Wang W, Nelson J, Bittman R, et al. NDRG1 functions in LDL receptor trafficking by regulating endosomal recycling and degradation. J Cell Sci 2013;126:3961–71.
[13] Kim KT, Ongusaha PP, Hong YK, Kurdistani SK, Nakamura M, Lu KP, et al. Function of Drg1/Rit42 in p53-dependent mitotic spindle checkpoint. J Biol Chem 2004;279:38597–602.
[14] Croessmann S, Wong HY, Zabransky DJ, Chu D, Mendonca J, Sharma A, et al. NDRG1 links p53 with proliferation-mediated

centrosome homeostasis and genome stability. Proc Natl Acad Sci U S A 2015;112:11583–8.
[15] Schweitzer CJ, Zhang F, Boyer A, Valdez K, Cam M, Liang TJ. N-Myc Downstream-Regulated Gene 1 Restricts Hepatitis C Virus Propagation by Regulating Lipid Droplet Biogenesis and Viral Assembly. J Virol 2018;92:e01117–66.
[16] Sevinsky CJ, Khan F, Kokabee L, Darehshouri A, Maddipati KR, Conklin DS. NDRG1 regulates neutral lipid metabolism in breast cancer cells. Breast Cancer Res 2018;20:55.
[17] Heller BA, Ghidinelli M, Voelkl J, Einheber S, Smith R, Grund E, et al. Functionally distinct PI 3-kinase pathways regulate myelination in the peripheral nervous system. J Cell Biol 2014;204:1219–36.
[18] Mao XY, Fan CF, Wei J, Liu C, Zheng HC, Yao F, et al. Increased N-myc downstream-regulated gene 1 expression is associated with breast atypia-to-carcinoma progression. Tumour Biol 2011;32:1271–6.
[19] Bandyopadhyay S, Pai SK, Gross SC, Hirota S, Hosobe S, Miura K, et al. The Drg-1 gene suppresses tumor metastasis in prostate cancer. Cancer Res 2003;63:1731–6.
[20] Mi L, Zhu F, Yang X, Lu J, Zheng Y, Zhao Q, et al. The metastatic suppressor NDRG1 inhibits EMT, migration and invasion through interaction and promotion of caveolin-1 ubiquitylation in human colorectal cancer cells. Oncogene 2017;36:4323–35.
[21] Bilbao JM, Schmidt RE. Genetically Determined Neuropathies. In: Bilbao JM, Schmidt RE, editors. Biopsy diagnosis of peripheral neuropathy. Cham: Springer International Publishing; 2015. p. 375–428.
[22] Mathis S, Goizet C, Tazir M, Magdelaine C, Lia AS, Magy L, et al. Charcot-Marie-Tooth diseases: an update and some new proposals for the classification. J Med Genet 2015;52:681–90.
[23] King RH, Tournev I, Colomer J, Merlini L, Kalaydjieva L, Thomas PK. Ultrastructural changes in peripheral nerve in hereditary motor and sensory neuropathy-Lom. Neuropathol Appl Neurobiol 1999;25:306–12.
[24] Matiasek K, Drogemuller C. Charcot-Marie-Tooth disease: inherited neuropathies revisited. Vet J 2011;188:254–5.
[25] Correard S, Plassais J, Lagoutte L, Botherel N, Thibaud J-L, Hédan B, et al. Canine neuropathies: powerful spontaneous models for human hereditary sensory neuropathies. Hum Genet 2019:138.
[26] Shelton G.D., Humphries N. What is the Complete Muscle Profile? 2017 [cited 25.10.2019]; Available from: http://vetneuromuscular.ucsd.edu/CompleteMuscleProfile.html.
[27] Skedsmo FS, Malachin G, Våge DI, Hammervold MM, Salvesen Ø, Ersdal C, et al. Demyelinating polyneuropathy in goats lacking prion protein. FASEB J 2020;34:2359–75.
[28] J. K Dyck PJ, Lais A, Lofgren EP, Stevens JC, et al. Pathologic alterations of the peripheral nervous system of humans. In: Dyck PJ, et al., editors. Peripheral neuropathy. Philadelphia: WB Saunders; 1984. p. 790–3.
[29] Walker TL, Redding RW, Braund KG. Motor nerve conduction velocity and latency in the dog. Am J Vet Res 1979;40:1433–9.
[30] Weller RO, Cervós-Navarro J. General Pathology of Peripheral Nerves. Pathology of peripheral nerves. London: Butterworths; 1977. p. 61–89.
[31] Summers BA, Cummings JF, DeLahunta A. Diseases of the Peripheral Nervous System. Veterinary neuropathology. St Louis, Mo: Mosby; 1995. p. 402–501.
[32] Braund KG, McGuire JA, Lincoln CE. Age-related changes in peripheral nerves of the dog. II. A morphologic and morphometric study of cross-sectional nerve. Vet Pathol 1982;19:379–98.
[33] Lassmann H, Ammerer HP, Kulnig W. Ultrastructural sequence of myelin degradation. Acta Neuropathol 1978;44:91–102.
[34] Galloway PG, Perry G, Gambetti P. Hirano body filaments contain actin and actin-associated proteins. J Neuropathol Exp Neurol 1987;46:185–99.
[35] Pareyson D, Scaioli V, Laura M. Clinical and electrophysiological aspects of Charcot-Marie-Tooth disease. Neuromolecular Med 2006;8:3–22.
[36] Hanemann CO, Gabreels-Festen AA. Secondary axon atrophy and neurological dysfunction in demyelinating neuropathies. Curr Opin Neurol 2002;15:611–15.
[37] Bilbao JM, Schmidt RE. Schwann Cells and Myelin in the Peripheral Nervous System. In: Bilbao JM, Schmidt RE, editors. Biopsy diagnosis of peripheral neuropathy. Cham: Springer International Publishing; 2015. p. 85–109.
[38] Kalaydjieva L, Nikolova A, Turnev I, Petrova J, Hristova A, Ishpekova B, et al. Hereditary motor and sensory neuropathy–Lom, a novel demyelinating neuropathy associated with deafness in gypsies. Clinical, electrophysiological and nerve biopsy findings. Brain 1998;121(Pt 3):399–408.
[39] Baethmann M, Göhlich-Ratmann G, Schröder JM, Kalaydjieva L, Voit T. HMSNL in a 13-year-old Bulgarian girl. Neuromuscul Disord 1998;8:90–4.
[40] Ricard E, Mathis S, Magdelaine C, Delisle MB, Magy L, Funalot B, et al. CMT4D (NDRG1 mutation): genotype-phenotype correlations. J Peripher Nerv Syst 2013;18:261–5.
[41] Bostock H, et al. Internodal Conduction Along Undissected Nerve Fibers in Experimental Neuropathy. In: Dyck PJ, et al., editors. Peripheral neuropathy. Philadelphia: W.B. Saunders; 1984. p. 900–10.
[42] Tazir M, Hamadouche T, Nouioua S, Mathis S, Vallat J-M. Hereditary motor and sensory neuropathies or Charcot–Marie–Tooth diseases: an update. J Neurol Sci 2014;347:14–22.
[43] Schochet SS Jr, McCormick WF. Ultrastructure of Hirano bodies. Acta Neuropathol 1972;21:50–60.
[44] Samanta J, Salzer JL. Myelination: actin disassembly leads the way. Dev Cell 2015;34:129–30.
[45] Goebbels S, Oltrogge JH, Wolfer S, Wieser GL, Nientiedt T, Pieper A, et al. Genetic disruption of Pten in a novel mouse model of tomaculous neuropathy. EMBO Mol Med 2012;4:486–99.
[46] Jung J, Cai W, Lee HK, Pellegatta M, Shin YK, Jang SY, et al. Actin polymerization is essential for myelin sheath fragmentation during Wallerian degeneration. J Neurosci 2011;31:2009–15.
[47] Vaquié A, Sauvain A, Duman M, Nocera G, Egger B, Meyenhofer F, et al. Injured Axons Instruct Schwann Cells to Build Constricting Actin Spheres to Accelerate Axonal Disintegration. Cell Rep 2019;27 3152-3166.e7.
[48] Duncan ID. Hammang JPJJoN. Ultrastructural observations of organelle accumulation in the equine recurrent laryngeal nerve 1987;16:269–80.
[49] Cooper BJ, Duncan I, Cummings J, de Lahunta A. Defective Schwann cell function in canine inherited Hypertrophic Neuropathy. Acta Neuropathol 1984;63:51–6.
[50] Luigetti M, Taroni F, Milani M, Del Grande A, Romano A, Bisogni G, et al. Clinical, electrophysiological and pathological findings in a patient with Charcot-Marie-Tooth disease 4D caused by the NDRG1 Lom mutation. J Neurol Sci 2014;345:271–3.
[51] Butinar D, Zidar J, Leonardis L, Popovic M, Kalaydjieva L, Angelicheva D, et al. Hereditary auditory, vestibular, motor, and sensory neuropathy in a Slovenian Roma (Gypsy) kindred. Ann Neurol 1999;46:36–44.
[52] Colomer J, Iturriaga C, Kalaydjieva L, Angelicheva D, King RHM, Thomas PK. Hereditary Motor and Sensory Neuropathy-Lom (HMSNL) in a Spanish family: clinical, electrophysiological, pathological and genetic studies. Neuromuscul Disord 2000;10:578–83.
[53] Horn M, Baumann R, Pereira JA, Sidiropoulos PN, Somandin C, Welzl H, et al. Myelin is dependent on the Charcot-Marie-Tooth Type 4H disease culprit protein FRABIN/FGD4 in Schwann cells. Brain 2012;135:3567–83.
[54] Yao JK, et al. Lipid composition of normal and degenerating nerve. In: Dyck PJ, et al., editors. Peripheral neuropathy. Philadelphia: WB Saunders; 1984. p. 510–30.